Design of a Small Angle Scatterometer

Michael Burka

12 August 1989

Abstract

A design for a small angle scatterometer is presented. The signal-to-background performance of the instrument is analyzed for angles from specular of 10^{-5} radians and above. It is shown that measurement of scattering from superpolished mirrors at scattering angles of a few times 10^{-4} radians in a laboratory-scale apparatus is achievable.

1 Introduction

Optical surfaces contain imperfections at all scale lengths with amplitudes that are much less than an optical wavelength. These imperfections are a source of stray (scattered) light in optical systems, with the amplitude of the imperfections determining the amplitude of light scattering and the spatial distribution of the imperfections determining the angular distribution of scattered light.

The imperfections of an optical surface can be represented as a superposition of two dimensional gratings of varying spacings and amplitudes. The grating equation gives the spatial scale of imperfections which result in scattering at a given angle from the specular direction. For small angle scattering, with illumination at near-normal incidence, this may be written[1]

$$\theta_s \approx \lambda/d \tag{1}$$

where θ_s is the angle between the scattered ray and the specular direction, λ is the illuminating wavelength, and d is the relevant spatial scale of imperfections. The intensity of radiation scattered at this angle is

$$I(\theta_s) \approx (ka\cos\theta_i)^2 \tag{2}$$

[1] Church, et. al., *Relationship between Surface Scattering and Microtopographic Features*, Optical Engineering, v.18, n.2, 1979.

where a is the amplitude of imperfections corresponding to d and $k = 2\pi/\lambda$.

The measurement of scattering at a small angle θ_s from specular requires that the surface to be tested be illuminated with a spot at least as large as the spatial scale $d = \lambda/\theta_s$. This, in turn, requires an optical system that can provide appropriate illumination and that can collect and measure the resultant scattered light.

2 Overview of scatterometer operation

Figure 1 shows a schematic diagram of the proposed scatterometer. Light is incident on mirror M1 from a single-mode fiber. The distance l_1 between the fiber end and the mirror is chosen so that the spot radius at M1 is 0.5 centimeter. The focal length of M1 is chosen to make the beam waist position correspond to the test surface S. The angle between l_1 and l_2 is chosen to prevent shadowing of the beam by the fiber mount. The angle θ_2 between l_2 and the surface normal is chosen to be as small as possible without M1 and M2 interfering. The angle θ_3 is variable. When $\theta_3 = \theta_2$, the principal beam will be focused onto the receiver fiber. When $\theta_3 = \theta_2 + \delta\theta$, light scattered by surface S at an angle $\delta\theta$ from specular will be focused onto the fiber, but the principal beam will be focused away from the fiber, so only scattered light is measured. The receiver fiber carries light to a photomultiplier tube. The input light is chopped, and a lock-in amplifier measures the photomultiplier signal.

A background subtraction must be performed to minimize the systematic error. The background consists of light scattered from mirrors M1 and M2 and light introduced into the fiber due to wavefront distortions of the principal beam. The subtraction method consists of removing the test optic and swinging the receiver arm so that light is measured at small angles from the beam axis (see Figure 2). When the test surface is flat, this is straightforward. When the test surface is curved, then the input conditions will have to be varied between the test measurement and the background subtraction measurement.

Measurements of scattering in transmission can be made with the apparatus configured as shown in Figure 3. The background subtraction is performed by removing the test piece and sweeping the receiver through the same range of angles. Again, this is straightforward if the faces of the piece are flat, otherwise, adjustments are required.

3 Choice of components and component separations

The divergence angle of the beam emitted by a single mode fiber is inversely proportional to the core diameter. To minimize spherical aberration in the system, it is desireable to have the smallest possible divergence angle. The largest core fiber which we know to be reliably single mode[2] is a fiber made by Eotech with a core diameter of 12.5 microns and a cladding diameter of 125 microns. This is the fiber we propose to use in the scatterometer. It has a beam divergence angle of 2.6×10^{-2} radians at an optical wavelength of .515 microns.

Having chosen the fiber, the requirement that the spot radius be one half centimeter dictates that mirror M1 have a focal length of about 19 cm. If we choose the same fiber for both input and output, then mirror M2 will also have a focal length of 19 cm.

The arm lengths l_2 and l_3 are largely irrelevant. The divergence angle of a beam with a half centimeter ω is $\approx 3.3 \times 10^{-5}$ radians, and the scattering angle of interest is only a few times larger. Thus, the wavefront seen by the receiver looks the same regardless of the length of l_3, provided it is less than 100 meters or so. In this proposal, l_2 is chosen to be 50 cm and l_3 to be 100 cm. These choices are a matter of convenience. At 100 cm, as the measured scattering angle is increased, the receiver mirror and fiber will move by fractions of a millimeter between data points.

4 Signal and backgrounds estimates

In the calculations in this section it is assumed that the light fiber used as the collector is a single mode fiber with the same core radius as the input fiber. Also, wavefront deformation due to optical aberration is neglected; aberrations are discussed in a later section. The assumption of a single mode fiber is made for ease of calculation. Multi-mode fibers typically propagate of order one hundred modes, and the calculation of their overlap with an incident beam is complicated. When the scatterometer is built we anticipate that tests will be performed with both single mode and multi-mode fibers at the output to see which performs better. The multi-mode fiber will offer less rejection of the principal beam, but it will collected more scattered light.

[2] Ken Shine, *Characterization of Large Core Single Mode Optical Fibers*, MIT Senior Thesis, 1985.

4.1 Sensitivity to light scattered from S

When the scatterometer receiver arm is rotated an angle $\delta\theta$ away from the direction of the main beam it receives light scattered by the surface S into a solid angle Ω_S around the angle $\delta\theta$. The size of Ω_S is given by

$$\Omega_S = \frac{\lambda^2}{\pi\omega_0^2} \tag{3}$$

where λ is the optical wavelength and ω_0 is the spot radius at S. In this system $\Omega_S = 3.4 \times 10^{-9}$ steradians. The opening half-angle of a cone which subtends this solid angle is 3.3×10^{-5} radians.

Neglecting the aberration in the focusing optics, the scattered light power incident on the fiber is

$$P_S = \frac{1}{P_{inc}} \frac{dP}{d\Omega}(\delta\theta)\,\Omega_S \tag{4}$$

where P_{inc} is the light power incident on S and $\frac{1}{P}\frac{dP}{d\Omega}$ is the BRDF.

4.2 Sensitivity to scattered light from M1 and M2

The analysis of the section above is applicable to M1.

$$P_{M1} = \frac{1}{P_{inc}} \frac{dP}{d\Omega}(\delta\theta)\,\Omega_S \tag{5}$$

The situation for M2 is different (see Figure 4). As the receiver arm is moved, the angle between the reflected principal beam and the fiber optic axis increases faster than $\delta\theta$. Specifically,

$$\delta\theta' = \left(\frac{l_3}{f_2} - 1\right)\delta\theta \tag{6}$$

where l_3 is the distance from S to M2 and f_2 is the focal length of M2. Since BRDF functions usually decrease with increasing angle, this means that the instrument is less sensitive to light scattered from M2 than light scattered from M1.

$$P_{M2} = \frac{1}{P_{inc}} \frac{dP}{d\Omega}(\delta\theta')\Omega_S \tag{7}$$

4.3 Sensitivity to the principal beam

When the receiver arm is rotated by an angle $\delta\theta$, the focus of the principal beam is displaced from the tip of the receiver fiber by an angle

$$\delta\theta' = \left(\frac{l_3}{f_2} - 1\right)\delta\theta \tag{8}$$

and a distance

$$\delta x' = f_2\delta\theta \tag{9}$$

where f_2 is the focal length of M2 (see Figure 4). The fraction of the incident beam which will be propagated in the fiber in this case is given by

$$\eta = e^{-\left(\frac{4x'^2}{\omega_f^2} + \frac{\pi^2\omega_f^2\delta\theta^2}{\lambda^2}\right)} \tag{10}$$

where ω_f is the fiber core radius. For the proposed system,

$$\eta = e^{-9\times10^6\delta\theta^2} \tag{11}$$

4.4 Summary of signal vs. background

We wish to compare the anticipated scattering signal from S to the backgrounds from M1, M2, and the principal beam. To do this, we must assume a model for the BRDF, and the model we assume is

$$\frac{1}{P}\frac{dP}{d\Omega} = \frac{10^{-6}}{\theta^2} \tag{12}$$

This model is consistent with the total losses of supermirrors and with data collected by various people at larger angles, though it is by no means known to hold for the small angles of interest here.

The table below shows the scattered signal from S, the backgrounds, and the incoherent sum of the backgrounds as a function of angle. The values are the fraction of incident light power which couples into the receiver fiber.

θ (rad)	P_{M1}	P_{M2}	η	$P_{M1}+P_{M2}+\eta$	P_S
1×10^{-5}	3.4×10^{-6}	1.9×10^{-6}	9.1×10^{-1}	9.1×10^{-1}	3.4×10^{-5}
3×10^{-5}	3.8×10^{-6}	2.1×10^{-7}	4.4×10^{-1}	4.4×10^{-1}	3.8×10^{-6}
1×10^{-4}	3.4×10^{-7}	1.9×10^{-8}	1.2×10^{-4}	1.2×10^{-4}	3.4×10^{-7}
2×10^{-4}	8.5×10^{-8}	4.7×10^{-9}	2.3×10^{-16}	9.0×10^{-8}	8.5×10^{-8}
3×10^{-4}	3.8×10^{-8}	2.1×10^{-9}	6.6×10^{-36}	4.0×10^{-8}	3.8×10^{-8}
1×10^{-3}	3.4×10^{-9}	1.9×10^{-10}	$<10^{-100}$	3.6×10^{-9}	3.4×10^{-9}
3×10^{-3}	3.8×10^{-10}	2.1×10^{-11}	$<10^{-100}$	4.0×10^{-10}	3.8×10^{-10}
1×10^{-2}	3.4×10^{-11}	1.9×10^{-12}	$<10^{-100}$	3.6×10^{-11}	3.4×10^{-11}

If we assume that the background subtraction can be done to an accuracy of 1%, then the table implies that scattering can be measured at angles above 200 microradians.

5 Optical aberration

The analysis of Section 3 assumes no aberration in the system, but an exact ray trace of the system has shown that there are aberrations. We have examined the spherical aberration and astigmatism in the proposed system. The beam cross section will be elliptical. The optimum value of the focal length of M1 has not been determined, but for a particular value that is probably close to optimum, the eccentricity of the spot cross section is .2 at the test surface S, and .3 at M2. The aberration also manifests itself in the focusing of the rays in one plane at a point several millimeters away from the focus of the rays in the orthogonal plane.

The aberration results in broadening of the beam spot at its focus. This may reduce the rejection of the principal beam at small angles, and result in an increase in the smallest measureable scattering angle. The aberration also reduces the coupling of scattered light into the fiber.

A potential solution to the first of these problems is to choose a focal length of M2 which will cause the principal beam to be smeared only in the direction orthogonal to the plane of incidence. A second solution is to choose an aspheric surface for M2. An aspheric would increase the principal beam rejection as well as improve the coupling of scattered light into the fiber.

Aspheric reflectors do not suffer the third order aberrations that spherical mirrors do. However, the microroughness and surface figure qualities which we have come to expect from spherical mirrors are not available in aspherics. Ideally, one would use identical off-axis parabolic reflectors for both M1 and M2; there would be no wavefront aberration in such a system. However, since the sensitivity of the system to scattered light from M1 is greater than from M2 (see Equations 5 and 7) a preferable solution is to choose M1 spherical and choose M2 to be a surface which negates the aberration introduced by M1. In general, one cannot undo all of the third order aberration with a single aspheric surface, but certainly the astigmatism can be corrected.

The microroughness achievable in an aspheric mirror is of order 10 angstroms r.m.s., and the surface figure is good to $\lambda/2$. These values are about an order of magnitude worse than the best spherical mirrors, so the

BRDF is about two orders of magnitude bigger. Looking at the table in Section 4.4, we see that if P_{M2} is increased by 100, then the sum of the background signals is about 50 times the scattered light signal. The background subtraction must be done to 1% precision at all scattering angles.

6 Sources of noise

6.1 Scattering from dust and air

Rayleigh scattering in air does not limit the performance of the scatterometer at small angles. The Rayleigh scattering cross section is

$$\frac{d\sigma}{d\Omega} = k^4 \alpha^2 \rho \tag{13}$$

where $k = \frac{2\pi}{\lambda}$, α is the molecular polarizability, and ρ is the density of scatterers. The light scattered out of the beam is given by

$$P_{scat} = P_0 \left(1 - e^{-\sigma l}\right) \tag{14}$$

where l is the path length in air. Then,

$$\begin{aligned} \frac{1}{P}\frac{dP}{d\Omega} &= l\frac{d\sigma}{d\Omega} \\ &= 2.3 \times 10^{-6} \end{aligned} \tag{15}$$

where the value is for air at atmospheric pressure and a path length of 200 cm. This is comparable to supermirror scattering only for angles of hundreds of milliradians and above.

Dust particles do compromise system performance. In the MIT scattering setup one can see flashes due to dust both by eye and on the lock-in amplifier. For a high performance system one must operate in either an extremely clean environment or at a pressure low enough to allow the dust to settle. At a pressure in the range of 10^{-2} to 10^{-1} Torr, the mean free path will be much greater than the dust particle dimensions, and the dust will settle.

Proposed chamber layouts using a 24 inch diameter by 60 inch deep horizontal chamber are shown in Figure 5. In any given configuration, the receiver arm will be moved by motorized micrometers. However, we do not expect to have a vacuum chamber large enough to move the apparatus from one configuration to another without opening the chamber and moving the components manually.

6.2 Dark current in the photomultiplier

The required incident power is determined by the need to have a signal on the photomultiplier which is larger than the shot noise from its dark current. A typical photomultplier may have an average of ten dark current electrons per second. Then

$$n(f) = (2\times < \dot{n} >)^{\frac{1}{2}} \tag{16}$$

and the r.m.s. noise power is given by

$$P_{rms} = \frac{h\nu n(f)}{\eta\sqrt{t_{int}}} \tag{17}$$

where h is Planck's constant, ν is the optical frequency, η is the quantum efficiency of the photomultiplier, and t_{int} is the integration time. If we assume a one second integration and a quantum efficiency of .2, then, for green light, $P_{rms} < 10^{-17}$ Watts. If we assume a factor of two loss in coupling to the fiber, then the incident power required to measure small angle scattering is less than a nanowatt. More power is required at large angles if the same receiver optics are used, but at large angles one has the freedom to use a receiver that collects light from a larger solid angle, because rejection of the principal beam is not a problem. It should also be noted that the light does not have to be comprised of a single longitudinal frequency of the laser cavity. In summary, light power is not a limiting factor in the scatterometer.

7 Cost and time estimate

A breakdown of anticipated costs is as follows:

- Laser. The Spectra-Physics 165 laser is adequate for the scatterometer. If the 165 tube dies, then a replacement tube will cost $6,500.
- Fiber. We have a sufficient quantity of optical fiber. We will require fiber chucks and related hardware at a cost of about $2,000.
- Mirrors. The mirrors used must be of exceptional quality in terms of microroughness and figure error, so that scattering from them does not dominate scattering from the test surface. The cost of a supermirror polishing run is about $3,000. The cost of coating is $2,000 per run, though these mirrors can be piggy-backed onto other coating runs.

If an aspheric surface is required for M2, then it will cost \$3,000 to \$5,000. An aspheric mirror would have a metal surface, and would not require coating. The total cost for mirrors will be \$5,000 to \$10,000.

- Photomultiplier. The cost of a photomultiplier tube is \$400. If a power supply cannot be scrounged from the lab, then it will cost \$2,000.
- Lock-in amplifier. We have lock-in amplifiers.
- Chopper. \$1,000.
- Vacuum system. It will be much less expensive to purchase a surplus vacuum tank from McGrath, or someone similar, and to modify it than it would be to build a new chamber from scratch. The McGrath catalog shows surplus chambers of sufficient volume in the \$7,500 range, and we guess that an additional \$5,000 will be required for modifications, flanges, etc. The required vacuum of 10^{-2} Torr is achievable with a mechanical pump. A liquid nitrogen trap will be required to prevent oil from backstreaming into the system.
- Mounting hardware. We will have to purchase several translation stages, including one motorized stage. \$3,500. Other hardware will be built in our shop.

The total system will cost between \$25,000 and \$36,000, based upon the final choice of optics, whether a photomultiplier power supply must be purchased, and whether the 165 laser tube requires replacement.

The components which require the greatest amount of time to procure are the vacuum enclosure and the mirrors. Let us assume that four months are required for the vacuum enclosure. The mirrors are likely to take longer, but initial assembly of the scatterometer can be done with off-the-shelf optics. Construction of the hardware will require about three months, and making the optics work will take another month. So, we estimate that a small angle scattering measurement capability can be established in eight months.

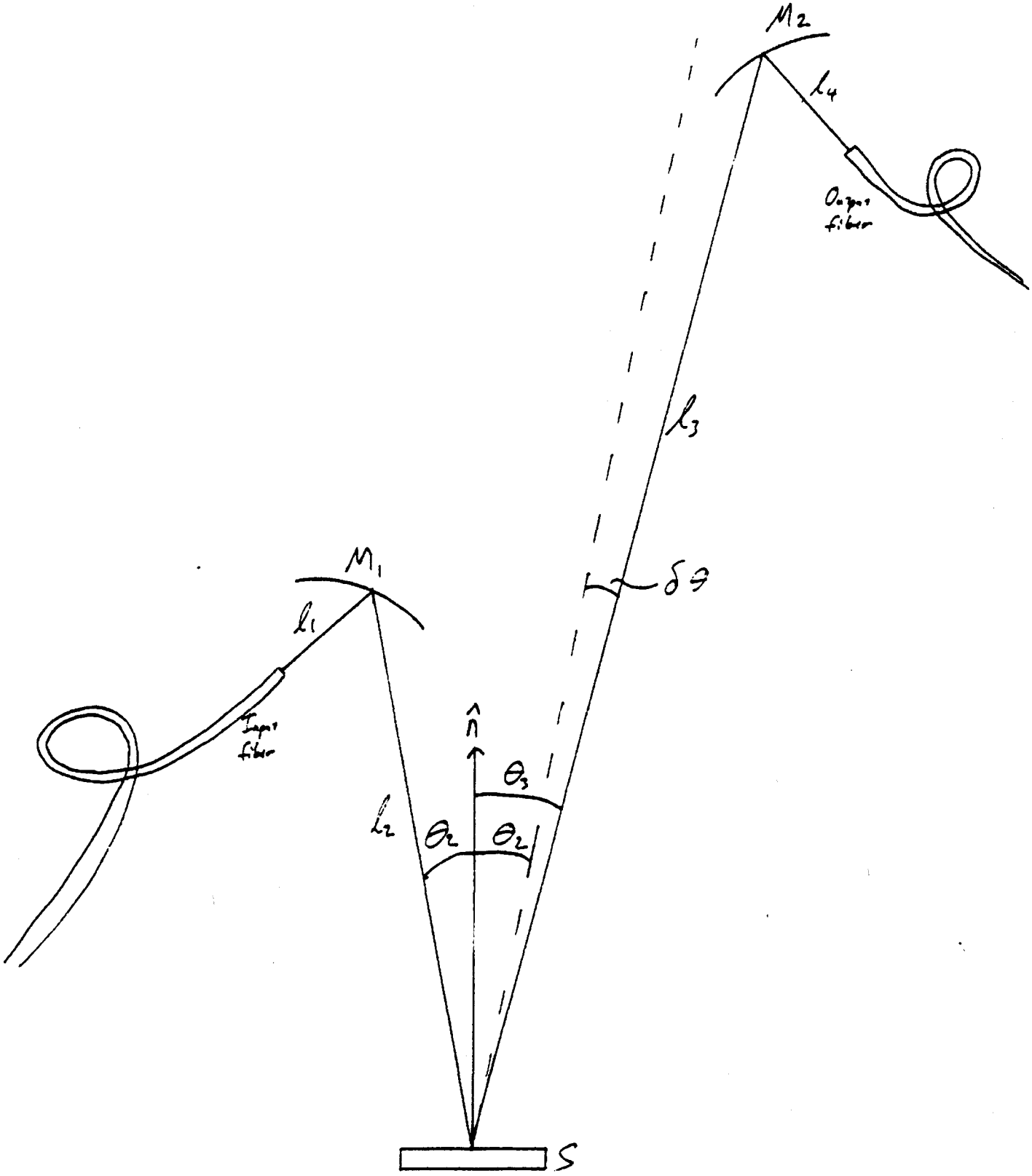
M_2
l_4
Output fiber
l_3
M_1
$\delta\vartheta$
l_1
Input fiber
$\hat{n}$
θ_3
l_2
θ_2
θ_2
S

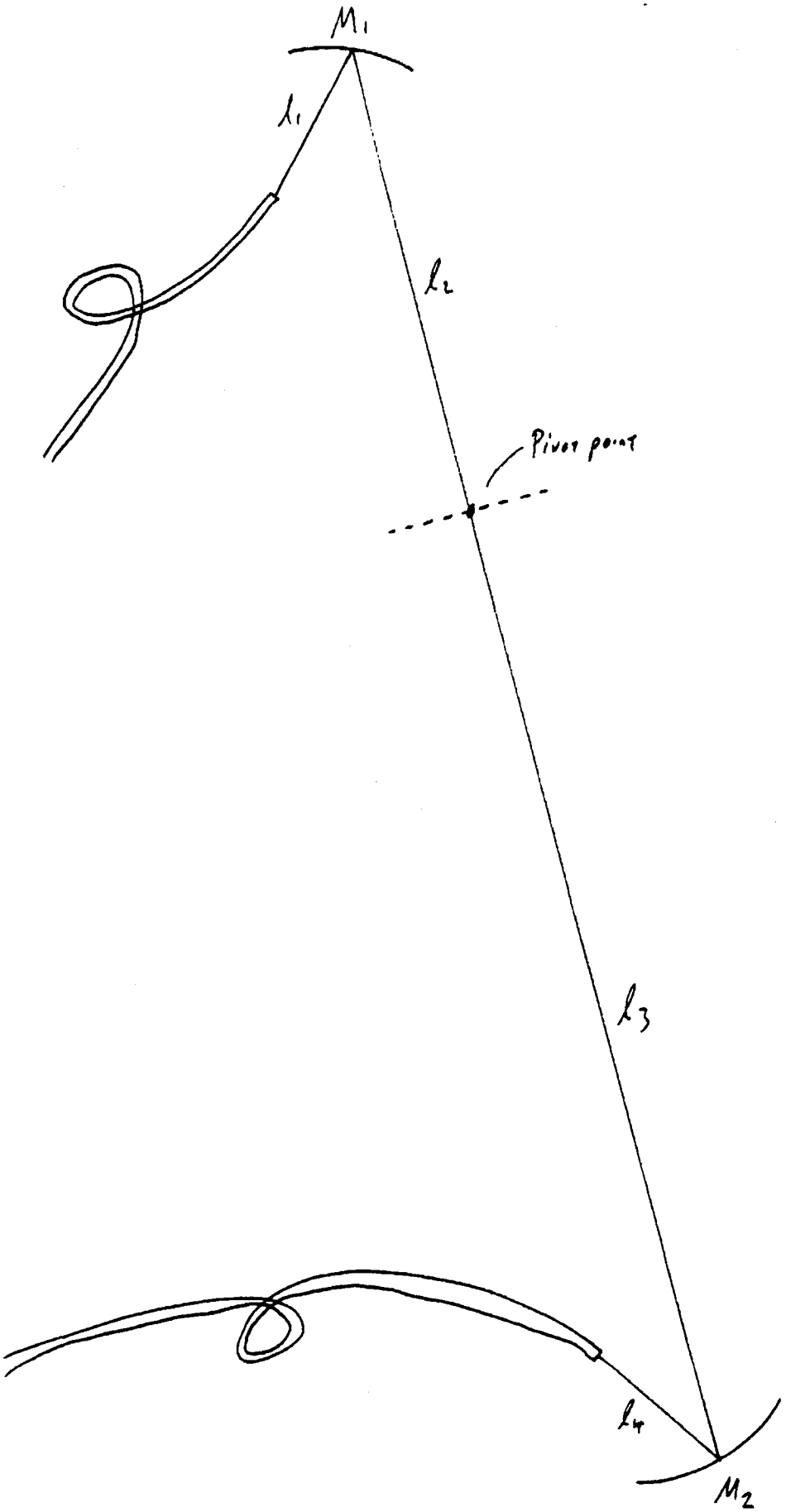
M_1
l_1
l_2
Pivot point
l_3
l_4
M_2

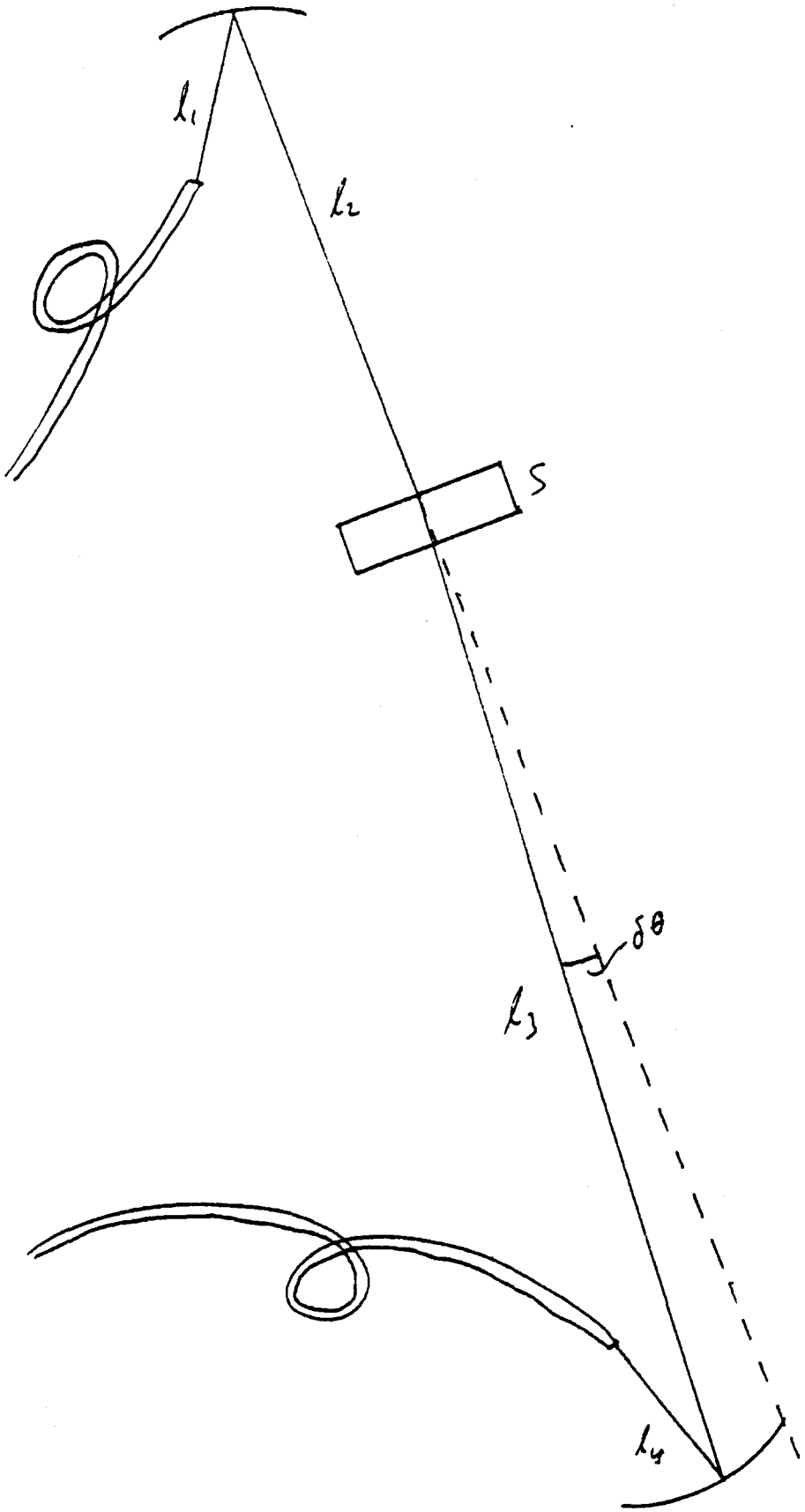
l_1
l_2
S
$\delta\theta$
l_3
l_4

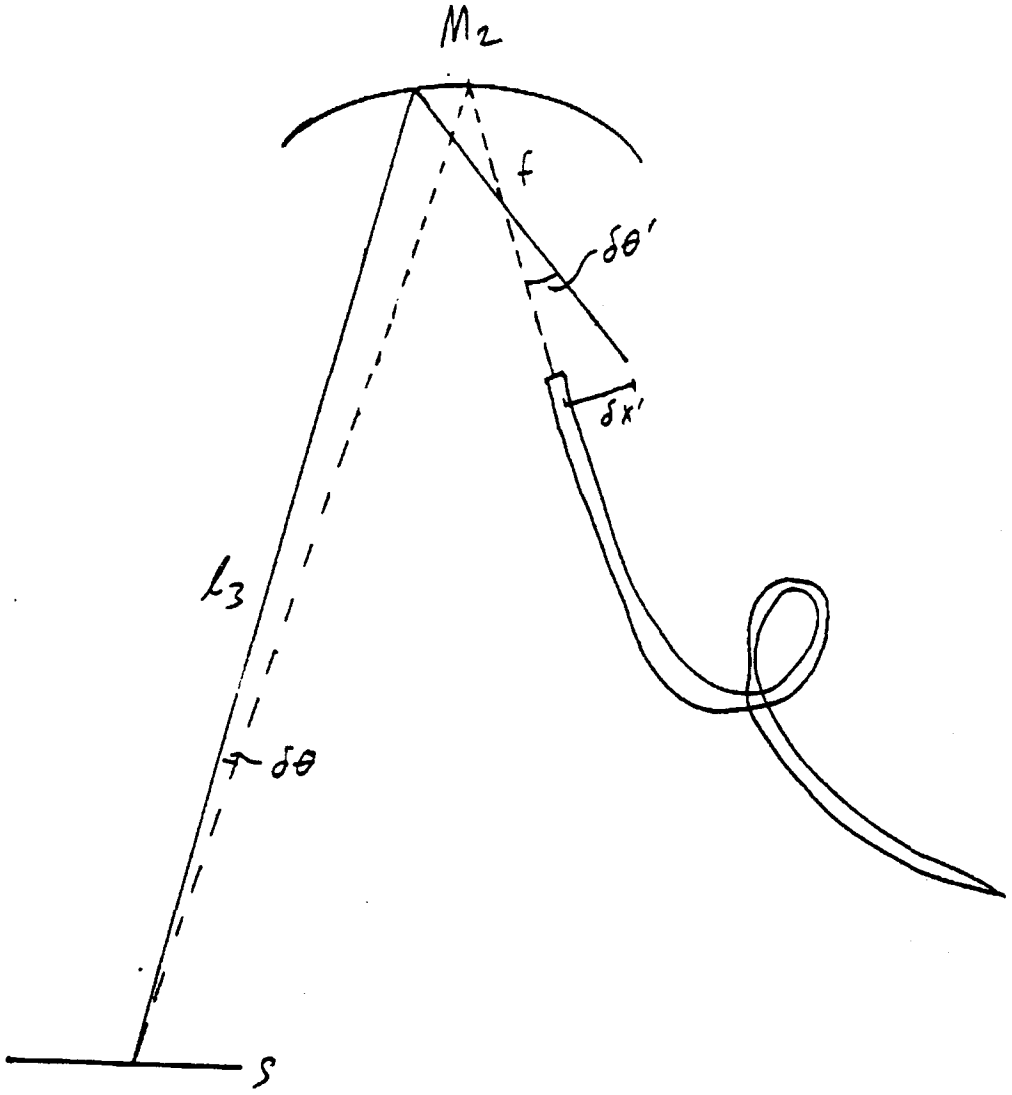

Figure 4

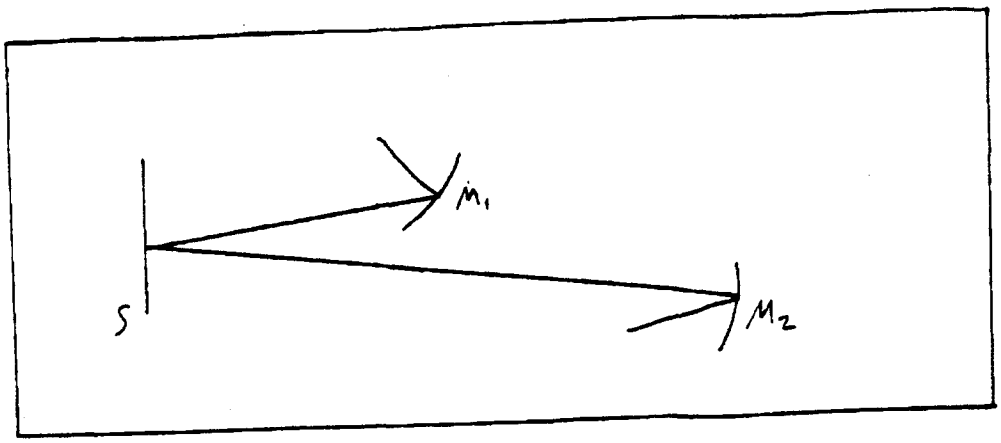

Reflection Measurement

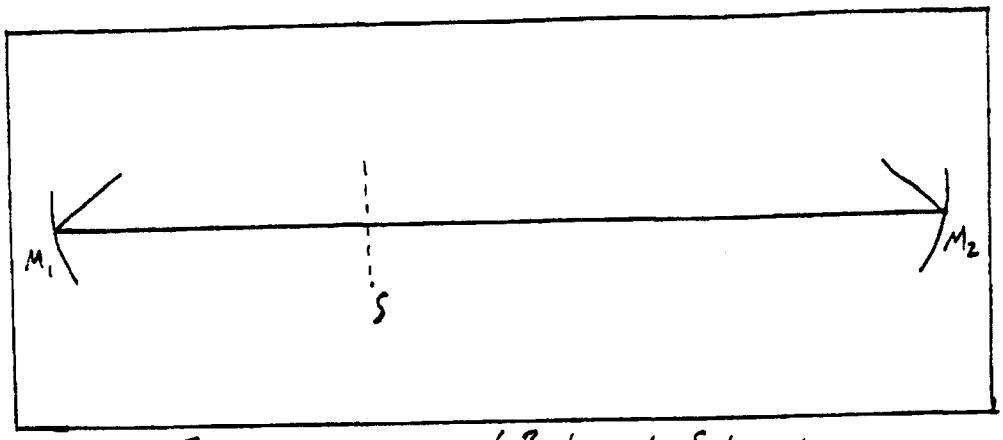

Transmission Measurement / Background Subtraction

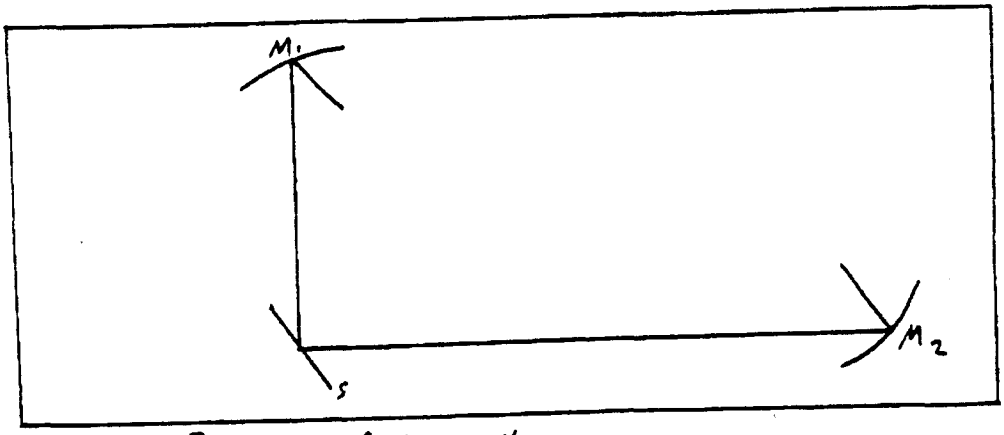

Beamsplitter Reflection Measurement

Figure 5